



On the intermittency of orographic gravity wave hotspots and its importance for middle atmosphere dynamics

Ales Kuchar¹, Petr Sacha^{2,3}, Roland Eichinger^{4,5}, Christoph Jacobi¹, Petr Pisoft², and Harald E. Rieder³

¹Institute for Meteorology, Universität Leipzig, Stephanstr. 3, 04103 Leipzig, Germany

²Department of Atmospheric Physics, Faculty of Mathematics and Physics, Charles University, V Holesovickach 2, 180 00 Prague 8, Czech Republic

³Institute of Meteorology and Climatology, University of Natural Resources and Life Sciences, Vienna (BOKU), Gregor-Mendel-Strasse 33, 1180 Vienna, Austria

⁴Meteorological Institute, Ludwig-Maximilians-University (LMU), Munich, Germany

⁵Deutsches Zentrum für Luft- und Raumfahrt (DLR), Institut für Physik der Atmosphäre, Oberpfaffenhofen, Germany

Correspondence: ales.kuchar@uni-leipzig.de

Abstract. When orographic gravity waves (OGWs) break, they dissipate their momentum and energy and thereby influence the thermal and dynamical structure of the atmosphere. This OGW forcing mainly takes place in the middle atmosphere. It is zonally asymmetric and strongly intermittent. So-called 'OGW hotspot regions' have been shown to exert a large impact on the total wave forcing, in particular in the lower stratosphere (LS). Motivated by this we investigate the asymmetrical distribution of the three-dimensional OGW drag (OGWD) for selected hotspot regions in the specified dynamics simulation of the chemistry-climate model CMAM (Canadian Middle Atmosphere Model) for the period 1979-2010. As an evaluation, we first compare zonal mean OGW fluxes and GW drag (GWD) of the model simulation with observations and reanalyses in the northern hemisphere. We find an overestimation of GW momentum fluxes and GWD in the model's LS, presumably attributable to the GW parameterizations which are tuned to correctly represent the dynamics of the southern hemisphere. In the following, we define three hotspot regions which are of particular interest for OGW studies, namely the Himalayas, the Rocky Mountains and East Asia. The GW drags in these hotspot regions emerge as strongly intermittent, a result that can also quantitatively be corroborated with observational studies. Moreover, a peak-detection algorithm is applied to capture the intermittent and zonally asymmetric character of OGWs breaking in the LS and to assess composites for the three hotspot regions. This shows that LS peak OGW events can have opposing effects on the upper stratosphere and mesosphere depending on the hotspot region. Our analysis constitutes a new method for studying the intermittency of OGWs, thereby facilitating a new possibility to assess the effect of particular OGW hotspot regions on middle atmospheric dynamics.

1 Introduction

Internal gravity waves (GWs) are a naturally occurring and ubiquitous phenomenon with large impact on the atmosphere's thermal and dynamical structure (Andrews and McIntyre, 1987; Fritts and Alexander, 2003). While the Brewer-Dobson circulation is believed to be driven mainly by Rossby waves, the mesospheric global circulation from the summer to the winter pole is dominated by GWs (Plumb, 2002; Alexander, 2013). GWs contribute to mesospheric cooling which often accompanies



Sudden Stratospheric Warmings (SSWs, Stephan et al., 2020) and they may also play an important role in vortex preconditioning (Albers and Birner, 2014).

In the current generation of general circulation models (GCMs), the resolution is usually too coarse to simulate GWs directly, requiring that the majority of their spectrum must be parameterized. Usually, two parameterization schemes are employed to distinguish between orographic (OGWs) and non-orographic GWs (NGWs). All GW parameterizations employ various degrees of simplification of GW sourcing, propagation and dissipation processes and contain certain tunable parameters that are only poorly constrained by observations. The performance of the schemes is commonly evaluated through comparison of zonal mean climatologies of GCMs and observations (Geller et al., 2013).

From observations, GWs are known to be distributed spatially asymmetric around the globe in so-called hotspots (e.g. Hoffmann et al., 2013). The asymmetry of the spatial distribution of the total GW drag (GWD) resulting from the two parameterizations is well represented by the OGW parameterizations (Šácha et al., 2018). OGWD hotspots are associated with well-known topographic structures such as the Andes and the Antarctic Peninsula in the southern hemisphere (SH), and the Rocky Mountains, the Scandinavian range and the Himalayas in the northern hemisphere (NH). These structures produce zonally asymmetric and interannually-variable torques, which significantly contribute to the total drag, emerging already as low as in the lower stratosphere (LS, Šácha et al., 2019).

Recent observational studies have shown that GW activity is highly intermittent (e.g. Hertzog et al., 2012; Wright et al., 2013) in terms of large amplitude wave-packets. In the present study, we focus on the valve layers in the LS (Kruse et al., 2016; Bramberger et al., 2017), where weak or zero horizontal winds between the subtropical jet and the polar night jet allow OGWs to break and deposit the momentum (and energy). As a first study of this kind, we will investigate the short-term variability of the three-dimensional (3D) OGWD in a GCM simulation. For this, we explore outputs of a transient CMAM (Canadian Middle Atmosphere Model, McLandress et al., 2013) simulation with specified dynamics. Our study starts with a model description, a short review of its evaluation and a brief description of other datasets used in the study in Section 2.1. In Section 2.2, we describe the methodology allowing to attribute the intermittency of parameterized OGWs, which leads to short (on a daily timescale) and strong bursts of localized wave forcing in the lower stratosphere. The simulated OGWD is compared with recent observational datasets in a traditional zonal mean monthly mean manner in Section 3.1. In Section 3.2 we present a statistical analysis of the OGWD within hotspots and analyze its intermittency. Finally, we present first results of a new method for studying the impact of spatiotemporally intermittent OGWD in Section 3.3, and end with concluding remarks in Section 4.

2 Data and methodology

2.1 Description of model and observations

The study is based on a simulation performed with the CMAM simulation (McLandress et al., 2013). CMAM is a chemistry-climate model with 71 vertical levels spanning from the surface up to $7 \cdot 10^{-4}$ hPa (about 100 km) with variable vertical resolution. It uses a triangular spectral truncation of T47, but the physical parameterizations are performed on a 3.75° horizontal grid. We selected a transient model simulation covering the period 1979–2010 with specified dynamics up to 1 hPa (referred



55 hereinafter as CMAM-sd). This means that Newtonian relaxation ("nudging") on spatial scales of $<T21$ to the 6-hourly horizontal winds and temperature time series from ERA Interim (Dee et al., 2011) is applied. For further details about the nudging we refer the reader to McLandress et al. (2014). The upper stratospheric discontinuities in the reanalysis data emerging in 1979, 1985, and 1998 have been removed from the model data using the procedure described in McLandress et al. (2014). CMAM-sd has been chosen for our analysis due to the freely accessible 6-hourly model data including 3D GW diagnostics, which to our
60 knowledge is currently unique in model data repositories. Moreover, CMAM is widely known for its realistic representation of middle atmospheric dynamics and has extensively been evaluated (see below).

In CMAM, OGWs and NGWs are parameterized using the schemes of Scinocca and McFarlane (2000) and Scinocca (2003), respectively. While McLandress et al. (2013) extensively detail both parameterization configurations, a brief outline of the parameterizations is given below. The OGW scheme launches two vertically propagating zero-phase-speed waves with orientation and magnitude depending on the near-surface static stability, wind speed and direction relative to the subgrid topography (anisotropic effects). Two tunable parameters exist in this parameterization scheme: the integrated radial dependence of the pressure drag ($G(y) = 0.65$) scaling the total vertical flux of horizontal momentum and the inverse critical Froude number ($Fr_{crit} = 0.375$) determining the breaking height that have been tuned to reduce warm temperature biases in the SH climatology (Scinocca et al., 2008). The NGWD scheme considers a spectrum of non-zero phase speed GWs propagating horizontally
65 into four cardinal directions at the fixed launch level (~ 125 hPa) with a pre-defined launch flux ($\sim 10^{-4}$ Pa). These parameters are tuned to exert a reasonable drag in the upper stratosphere and mesosphere (McLandress et al., 2013).

CMAM-sd has been vastly evaluated by means of comparisons with observations (e.g. Shepherd et al., 2014). Climatology of zonal winds and temperatures in the lower to middle stratosphere in CMAM-sd have been found to be consistent with reanalyses and observations, although some local biases have been identified higher in the upper stratosphere and mesosphere (Shepherd
75 et al., 2014; Pendlebury et al., 2015; Kuilman et al., 2017).

In the first section of the results, we compare the OGWD of the CMAM-sd simulation with the most recent generation of NASA's reanalysis MERRA2 (Modern Era Reanalysis for Research and Applications-2) version of the Goddard Earth Observing System-5 (GEOS-5, Molod et al., 2015), the Japanese 55-year Reanalysis (JRA55, Ebita et al., 2011) and with the observation-based GW climatology dataset GRACILE (Ern et al., 2018). MERRA2 uses both orographic (McFarlane, 1987) and non-orographic (Garcia and Boville, 1994) wave parameterizations (see details in Fujiwara et al., 2017), while
80 JRA55 uses an OGW parameterization only (Iwasaki et al., 1989). GRACILE has been compiled with data from the SABER instrument on NASA's TIMED (Thermosphere Ionosphere Mesosphere Energetics Dynamics) satellite together with data from HIRDLS (High Resolution Dynamics Limb sounder) aboard NASA's Aura satellite. Note, SABER data are not assimilated in MERRA2. The GRACILE data set is suitable for comparison with GW distributions in global models either with parameterized or resolved GWs. GW momentum fluxes from SABER and HIRDLS have been used previously for comparison with selected
85 climate models and radiosonde observation by Geller et al. (2013).

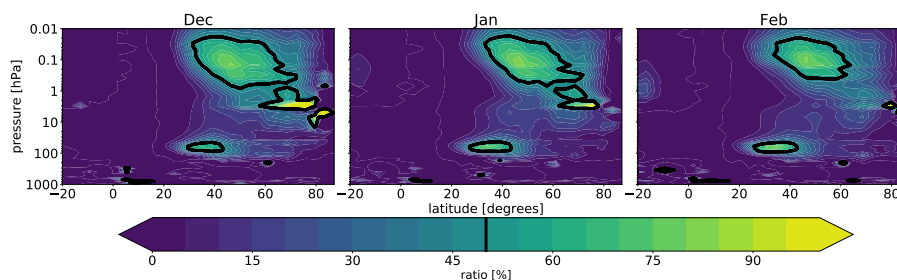


Figure 1. Ratio of zonally averaged OGWD in zonal direction (units: %) to the total wave forcing (resolved waves represented by EPFD + OGWD + NGWD) for the climatological average of the period 1979-2010. The black contour represents 50% contribution of OGWD.

2.2 Construction of hotspot composites

Figure 1 shows the boreal winter (DJF) average of the zonal-mean OGWD contribution to the total (OGWD+NGWD+resolved wave drag represented by Eliassen-Palm flux divergence (EPFD)) zonal mean wave drag in the NH in CMAM-sd. Here two regions emerge in the middle atmosphere where the OGWD dominates the net drag, namely the lower mesosphere and the LS. In the lower mesosphere, OGWD controls most of the net drag between 40 and 75°N in all months with the exception of the boreal summer months (not shown). In the LS between 25 and 50°N, OGWD constitutes the majority of the net drag during boreal winter and adjacent spring and autumn months. The region of the LS OGWD maximum in the extratropics at 70 hPa starts at the upper flank of the subtropical jet and extends into the area of weak winds below the polar night jet. According to theoretical considerations postulated in Teixeira (2014) or following observational evidence from lidar measurements (Ehard et al., 2017), these areas, known as the valve layers (e.g., Kruse et al., 2016; Bramberger et al., 2017), are regions where weak or zero horizontal winds provide critical levels for OGWs. There, they break and deposit horizontal momentum. The dominance of the zonal mean OGWD forcing in the NH LS net drag emerges also as a robust feature in the free running simulations with global (chemistry) climate models (including CMAM, Šácha et al., 2019; Okamoto et al., 2011; Dietmüller et al., 2018). In reanalyses, GWD constitutes about half of the net forcing in the LS (Albers and Birner, 2014; Abalos et al., 2015; Sato and Hirano, 2019).

The dominant OGWD in the LS at 70 hPa is mostly distributed into hotspots connected with regions of distinct topography. In our analysis, we focus on the hotspots highlighted by the colored boxes in Fig. 2. The amber, purple and green boxes represent the Himalaya (HI, 70-102.5°E and 20-40°N), East Asia (EA, 110-145°E and 30-48°N) and West America (WA, 235-257.5°E and 27.5-52°N) hotspots, respectively. The HI and WA hotspot areas have been defined based on the mountain range locations. The definition of the EA hotspot is not that straightforward as it corresponds to a geographical location of multiple mountain ranges. Several studies have reported the importance of the EA region as a "vertical communicator" from the troposphere into the stratosphere (e.g. Nakamura et al., 2013; Cohen and Boos, 2017; White et al., 2018). Strong OGW activity in the LS in this region has also been shown in observations. Šácha et al. (2015) have highlighted peak GW activity

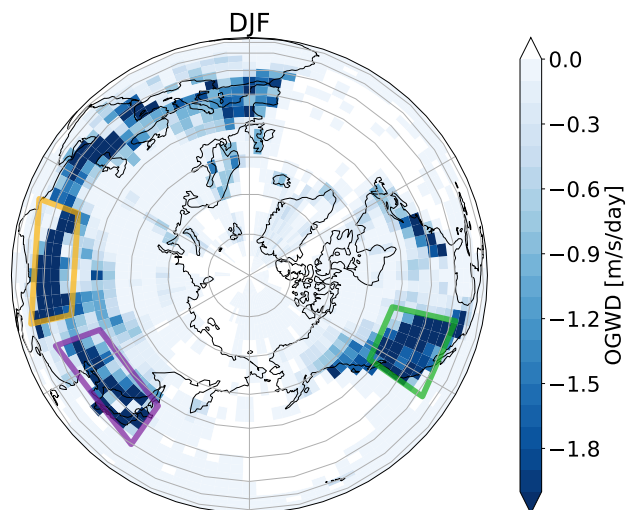


Figure 2. Boreal winter climatology of the zonal OGWD component [m/s/day] at 70 hPa over the period 1979-2010. The amber, purple and green boxes represent the Himalaya (70-102.5°E and 20-40°N), East Asia (110-145°E and 30-48°N) and West America (235-257.5°E and 27.5-52°N) hotspots, respectively.

110 in the LS in a pronounced localized region corresponding to the EA hotspot as defined here. Moreover, Pisoft et al. (2018) showed that this region is unique because the background winds provide here a critical line for wave propagation in the LS.

In order to analyze the CMAM-sd simulation with respect to the importance of asymmetrical GW forcing, we turn now to the analysis of these three hotspot regions. To create a representative OGWD time series for a particular hotspot, we area-weighted and averaged the OGWD at each grid point within the selected hotspots. With OGWD we refer here only to the zonal acceleration through OGWs, meridional accelerations were not analysed. For this type of analysis, we used daily mean values of the 6-hourly model data. The resulting OGWD time series for the three hotspot regions is shown in Fig. 3. The OGWD is generally small during summer and large during winter. In the parameterization the prevailing westward GWD is mainly determined by the near-surface wind speed and its direction relative to the orientation of the subgrid topography (McLandsres et al., 2013; Šácha et al., 2018). During winter, many peak OGWD events can be seen in all hotspot time series.

120 To characterize the intermittency of (strong) OGWD events, we apply a peak-detection algorithm to detect peaks (local minima) that exceed immediate neighbors with minimum distance of 20 days. Only the peaks with amplitude beneath the normalized threshold:

$$\text{threshold} = 0.55(\min \text{OGWD} - \max \text{OGWD}) + \max \text{OGWD} \quad (1)$$

are detected. Here, the factor 0.55 is a free parameter to assess relatively strong events. The normalized threshold accounting for the time series range is different for each GW hotspot, i.e. it is -6.66 m/s/day for the Himalayas, -5.07 m/s/day for East Asia and -7.13 m/s/day for West America, respectively. Note that those threshold values shown above represent the area-weighted average and even one order of magnitude larger values can be seen in individual grid points (see Section 3.2).

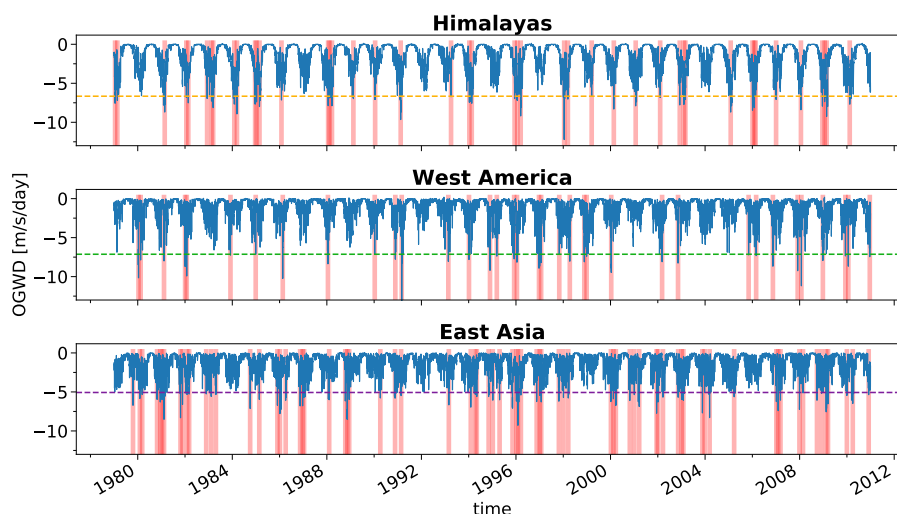


Figure 3. Area-weighted average of daily OGWD within the areas representing the Himalayas (upper panel), West America (middle panel) and East Asia (lower panel). Peak events separated by 20-day timescale are highlighted by pink bars (see main text for explanation). Horizontal dashed lines show the OGWD threshold of the peak detection algorithm. For greater detail we refer the reader to the interactive figures in the supplement.

The 20-day timescale was selected to be consistent with the definition of a simplified version of the World Meteorological Organization (WMO) criteria using the reversal of the winds at 60°N and 10hPa for SSW detection proposed by Charlton and Polvani (2007) and split and displacement SSW events employed in Seviour et al. (2013), respectively. The identification of strong OGWD events allows us to calculate composite anomalies of different variables by subtracting daily values from the monthly long-term climatology. The monthly climatology excludes months where SSW split and displacement events occurred according to the criteria of Seviour et al. (2013). The statistical significance of the composites was derived through application of a bootstrap method based on 10000 samples. The relative change of the particular variable was averaged according to the days preceding the identified peak events (lags from -10 to -1) and the days following the identified peak events (lags from +1 to +10).

3 Results

3.1 Evaluation of zonal mean GW diagnostics

We carry out comparisons of zonal mean GW parameterization outputs with observations to classify GW representation in CMAM-sd in relation to former validation efforts (Geller et al., 2013). A comparison of zonal mean absolute GW momentum fluxes from GRACILE and CMAM-sd is shown in Fig.4. We analyze explicitly the sum of both GW fluxes (OGWs and NOGWs), because it is impossible to derive pure OGW momentum fluxes from satellite observations. We restrict the analysis to



boreal winter months in the lower and middle stratosphere, i.e. at 20 km and 30 km, respectively. These are the closest levels to the LS OGWD maxima in the NH extratropics (see Fig. 1) and the two lowest altitudes available from GRACILE for HIRDLS and SABER, respectively. Figure 4 shows that GW momentum fluxes in CMAM-sd largely overestimate the values from GRACILE between 30 and 60°N in November, December and January at both levels. The shading represents climatological maxima or minima, which denotes the natural variability during the time periods used for averaging. In February, the modelled fluxes drop to much lower amplitudes at 30 km, which largely improves the agreement with the observations. However, the CMAM-sd fluxes in February still exceed those from observations by a factor of 2. While the meridional flux distributions of GRACILE reveal maxima around 50°N, the CMAM-sd fluxes show a latitudinal structure with multiple maxima between 40 and 70°N. At lower latitudes observations show larger and non-zero fluxes compared to the values produced in the CMAM-sd parametrizations, especially at 20 km.

In their Fig. 2, Geller et al. (2013) reveal that CMAM-sd agrees well in terms of latitudinal GW variation but overestimates absolute GW momentum fluxes in the NH compared with other models. Geller et al. (2013) also documented in their Fig. 1 that absolute GW momentum fluxes from HIRDLS or SABER are larger during winter in the SH than in the NH. Furthermore, they show a similar overestimation of fluxes by models for January 2006 in the NH, while for July 2006 in the SH, models agree better with the observations. A comparison of the austral winter climatology of CMAM-sd momentum fluxes with GRACILE in the SH leads to the same conclusion (better agreement of magnitude), especially north of 60°S (not shown). Those results underline the fact that the parametrization of OGWs in CMAM-sd is tuned to represent a missing drag in the SH (McLandress et al., 2012) resulting in the overestimation of the absolute GW momentum fluxes in the NH. We note that a similar effect of GW parameterizations has been recently documented for CESM1-WACCM4 (Garcia et al., 2017).

In Figure 5 we show a comparison of the net zonal-mean OGWD (blue line) and NGWD (orange line) from CMAM-sd and reanalyses (JRA55 (red line) and MERRA2 (black lines)) at 70 hPa (~ 18 km) in the NH, i.e. the region of the LS OGWD maximum (see Fig. 1). In comparison with reanalyses, CMAM-sd overestimates the net GWD by about a factor of two from 30 to 70°N. These are the latitudes where OGWD almost entirely determines the total GWD in CMAM-sd. However, when we add MERRA2 assimilation analysis increments to the GWD tendency similarly to Scheffler and Pulido (2015), MERRA2 still does not show as strong decelerations as CMAM-sd in the extratropical LS. The overestimation may stem from differences in OGWD parametrizations of MERRA2, JRA55 and CMAM-sd since the two-wave momentum flux representation in CMAM-sd leads to 30-50% more GW momentum flux up into the middle stratosphere than the single-wave representation (used in MERRA reanalyses, McFarlane, 1987), depending on the pressure level and season (Scinocca and McFarlane, 2000). After accounting for the analysis increment, MERRA2 (black dotted line) and JRA55 (red line), agree remarkably well in terms of both, amplitude and meridional distribution of the negative GWD, especially between 25-50°N. Positive GWD values in MERRA2 (black dotted line) at low and high latitudes can be interpreted as missing GWD from NGWs, which are typically launched with small amplitudes so that they deposit their momentum in the upper stratosphere and mesosphere (Kruse et al., 2016).

The climatological relative contribution of parameterized GWs to the resolved drag represented by the EPFD (see eq. S4) agrees well between CMAM-sd and MERRA2 and is slightly overestimated in JRA-55, albeit the GWD maximum (minimum

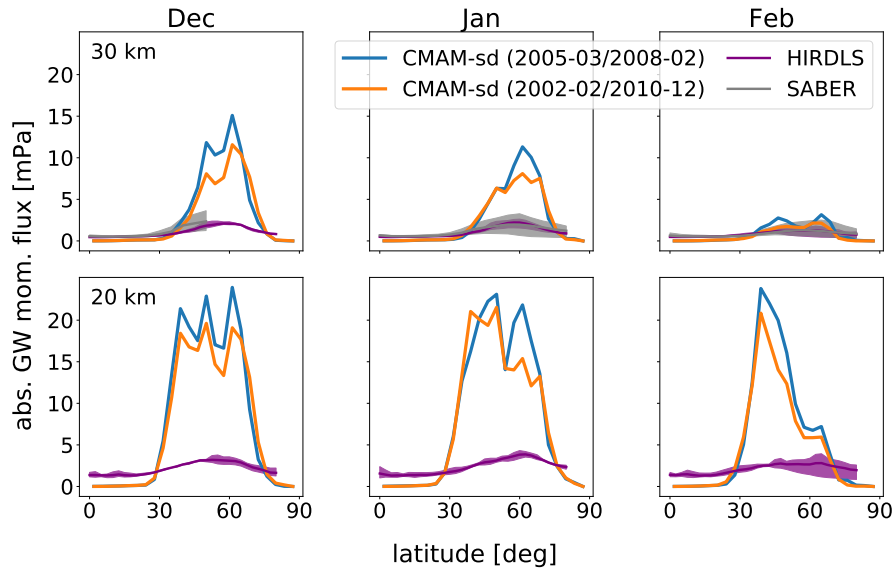


Figure 4. Climatologies for the absolute GW momentum fluxes [mPa] at 20 km (lower panels) and 30 km (upper panels) from CMAM-sd averaged over the HIRDLS period (Mar 2005 – Feb 2008), over the longer period (Feb 2002 – Dec 2010), respectively, and from SABER. The shading represents climatological maxima or minima adopted from the GRACILE dataset.

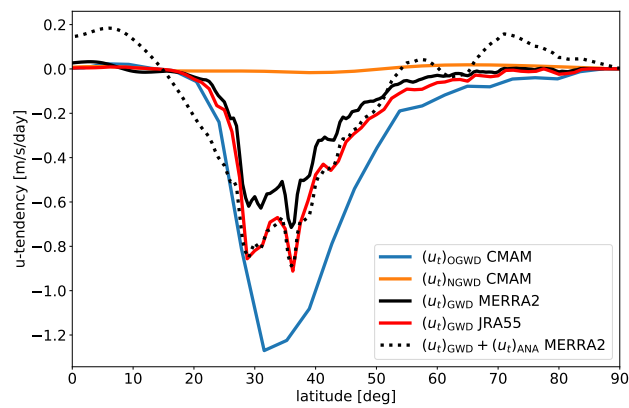


Figure 5. Climatology of total parametrized zonally averaged GWD [m/s/day] at 70 hPa in January averaged over the period 1980–2010. The black solid line represents the MERRA2 tendency of eastward wind due to GWD and the black dotted line with the additional tendency of eastward wind from assimilation analysis, respectively. The red line represents the JRA55 tendency of eastward wind due to GWD. The blue and orange lines represent the CMAM-sd tendencies of eastward wind due to OGWD and NGWD, respectively.



of EPFD) being shifted to higher latitudes in CMAM-sd (see Fig. S1 in the supplement). This suggests that while GWD in reanalyses is underestimated (Kruse et al., 2016), the resolved wave forcing may compensate the parametrized GWD (van Niekerk et al., 2018). In reanalyses the residual term of the zonal-mean momentum budget is still present in the LS (e.g. for JRA-55 see Fig. 2 in Martineau et al., 2016; Seviour et al., 2012, for ERA-Interim). NGWD is almost zero at 70 hPa in CMAM-sd and the residual term has a double-peak structure (see Fig. S2), which may stem from missing NGWs generated from atmospheric jets and fronts (Plougonven and Zhang, 2014; Chun et al., 2019) or underestimated OGWD (Seviour et al., 2012).

185 In summary, from the traditional zonal mean, monthly mean perspective we have shown that the OGW fluxes and drag in CMAM-sd are overestimated in the NH LS in comparison to observations and reanalyses, respectively. These biases have to be kept in mind in the following analysis and in the discussion of the results. In the next section we show that the OGW flux and drag cannot be fully described by the zonal mean quantities because they are strongly alternating in time and space.

3.2 Intermittency

190 The CMAM-sd OGWD spatial distribution is zonally asymmetric, which can be seen in Fig. 2 and in Šácha et al. (2018). In this section, we analyze the distribution of the OGWD magnitude in the three selected NH hotspots (HI, EA and WA). Figure 6 shows the probability density function of the OGWD magnitude for the three hotspots at 70 hPa during boreal winter. The probability density is computed from the spatially averaged OGWD over the whole hotspot (blue columns) and from the unaveraged OGWD time series of all grid boxes within the hotspot location (amber for HI, green for EA and purple for WA).
195 Dashed vertical lines show the value of the 10th and the 1st percentiles for the unaveraged times series and the solid vertical line indicates a threshold OGWD value that is later in the manuscript used to construct the composites of strong events for spatially averaged OGWD within the hotspots (see Section 3.3 below).

Figure 6 shows that the averaged OGWD values reach maxima around -10 m/s/day. The probability distributions for the EA and WA hotspots roughly follow a log-normal distribution. In the WA hotspot, positive OGWD values occur relatively
200 frequently. This leads to the fact that the distribution is not log-normal over the whole range. The threshold for strong OGWD events is largest for WA and smallest for EA.

In the spatially not averaged data we observe much broader tails of the probability density distribution and OGWD values reach up to -90 m/s/day in HI and -75 m/s/day in EA and WA. However, for WA, OGWD events larger than 50 m/s/day are rare in comparison to EA and especially HI. This is also reflected in the position of the 10th and 1st percentile, which have
205 the largest value for the HI hotspot. The 10th percentile is at approximately 6 m/s/day for both EA and WA hotspots, but the 1st percentile is connected with a somewhat stronger OGWD for EA in comparison to WA (-19.5 m/s/day). Surprisingly, the second most frequent OGWD value is a small positive drag for all hotspots, for WA we find in addition some less frequent positive drags up to 5 m/s/day.

On the basis of recent observational studies (e.g. Hertzog et al., 2012; Wright et al., 2013), the intermittency of GWs has been
210 increasingly acknowledged. Large GW events are known to be highly intermittent, which can be well quantified (Plougonven et al., 2013) by the so-called Gini coefficient (Gini, 1912, the coefficient varies between 0, meaning a constant series without

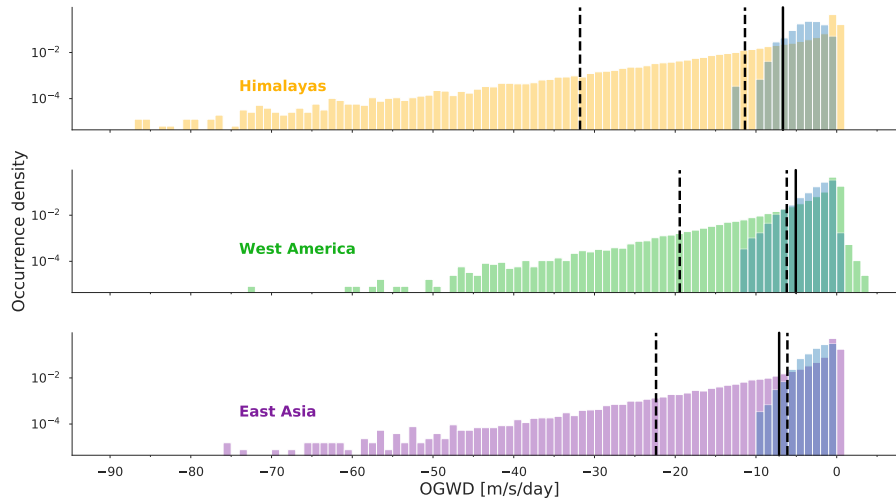


Figure 6. Daily OGWD distribution at 70 hPa during boreal winter within the Himalaya, East Asia and West America hotspot, respectively. Blue columns represent spatially averaged OGWD over the hotspot regions. Columns with different colors (amber for HI, green for EA and purple for WA) are unaveraged OGWD of all grid boxes within the hotspot regions, respectively. Vertical dashed lines show the value of the 10th and the 1st percentiles for the unaveraged OGWD. The vertical solid lines show the OGWD threshold of the peak detection algorithm (see Section 3.3).

intermittency and 1, meaning maximum intermittency) usually calculated for GW momentum fluxes. For an exponential distribution the Gini coefficient is 0.5 and for a log-normal distribution the value is dependent on the standard deviation (Kendall and Stuart, 1977, p. 48):

$$215 \quad \text{erf}(\sigma/2) = \frac{2}{\sqrt{\pi}} \int_0^{\sigma/2} \exp^{-t^2} dt. \quad (2)$$

The intermittency of OGW momentum fluxes in the atmosphere as well as of OGWD in the model is influenced by the sourcing processes as well as by the variability of the background flow during propagation. Figure 7 shows the annual cycle of the Gini coefficient for spatially averaged GW momentum fluxes over the hotspots (see Figs. S4–S11 for horizontal distributions of the Gini coefficient). In the upper to middle stratosphere (upper row in Fig. 7) the OGW fluxes are extremely intermittent with a weak annual cycle with maxima during boreal summer. In the LS, the Gini coefficient of the OGWs is smaller in the boreal winter months for all hotspots. Still, OGWs in the LS can be considered as highly intermittent (minimal Gini coefficient 0.5 ± 0.05). The three hotspot intermittencies of OGWD are comparable or slightly higher than estimated for OGW momentum fluxes from observations above regions with distinct topography (although for the SH) ranging from 0.35 to 0.8 for the Antarctic Peninsula (Alexander et al., 2016; Jewtoukoff et al., 2015; Plougonven et al., 2013; Wright et al., 2013). Especially for OGWs in the upper stratosphere, the calculated Gini coefficients largely resemble the log-normal distribution estimate according to Eq. 2 (see Figs. S12–13). This is in agreement with the studies by Hertzog et al. (2012) and Plougonven et al. (2013), who



found this relationship in balloon and spaceborne observations, and mesoscale numerical simulations. The intermittency of the hotspot regions is also clearly larger than the intermittency calculated from the NH mid-latitude (20–60°N) zonal mean GW fluxes ranging from 0.1 to 0.4 in the LS (gray lines in Fig. 7). In other words, a significant amount of the intermittency is lost
230 due to the zonal averaging of momentum fluxes. The Gini coefficient of the NH mid-latitude OGW fluxes shows the largest intermittency in spring and a secondary maximum in fall. This semiannual variation is larger with altitude and thus determined by the GW propagation conditions associated with the background atmosphere (Cao and Liu, 2016).

In the LS there are larger intermittency differences between the hotspots. During boreal winter, the lowest intermittency emerges for the EA hotspot. This can be connected with the fact that it involves multiple mountain ranges. The intermittency
235 of OGWD in the WA and HI remains high (minimally around 0.7) during the winter months. The annual cycle for WA is not as pronounced as for the other hotspots. The Gini coefficient in the LS slightly increases with altitude suggesting that lower stratospheric background flow variability (critical line occurrence, Doppler shifting) plays only a minor role. The momentum flux intermittencies in the LS and at 850 hPa are comparable (see Fig. S3), pointing towards an important contribution of near-surface variability. A similar result has been derived for variability at longer timescales (Šácha et al., 2018). Only the EA
240 hotspot reveals a weak annual cycle at 850 hPa suggesting that the annual cycle exposed for HI and WA in the stratospheric levels is determined by the background-flow variability.

The parameterized NGWD derived from spatially uniform fluxes at the launch level is also intermittent. Near the launch level in the LS (where NGWD is negligible) the Gini coefficient is about 0.1, but it increases with altitude and reaches 0.4 during boreal winter in the upper stratosphere (see dashed lines in Fig. 7). The low intermittency at lower altitudes is related
245 to uniform momentum fluxes at the launch levels. Higher above larger NGW intermittency arises due to vertical propagation through variable background winds especially in boreal winter. Note, the Gini coefficient would be higher and show a more pronounced seasonal variability if the GW parameterization in CMAM-sd was source related.

3.3 Composite analysis

In the previous sections we demonstrated that the OGWD is a zonally asymmetric and intermittent forcing that dominates the
250 total wave drag in the NH LS during the boreal winter. We propose a method for studying the OGWD influence by constructing strong-peak event OGWD composites of particular hotspots. To reduce the OGWD complexity we make the assumption that the OGWD inside a particular hotspot is homogeneous. Figs. 6 and 7 showed that spatial averaging inside the hotspots maintains the intermittent feature of the OGWD and only the information of the long tails of the distribution with extreme (and apparently very localized) drag values of -20 m/s/day is lost.

The number of days with detected peak events by the peak detection algorithm is shown in Table 1. For HI and WA the majority of detected strong OGWD events falls between November (December for HI) and March, for EA between September and May. Most of the events occur for all hotspots in January. To construct the composites we restrict the analysis to DJF, allowing us to assume a similar climatology for all peak events. Figure 8 shows the composites of the spatially averaged OGWD anomalies corresponding with strong OGWD events for each hotspot on the 20-day timescale. We note in passing that
260 we have analyzed these composites also with a 30-day timescale yielding practically identical results (not shown).

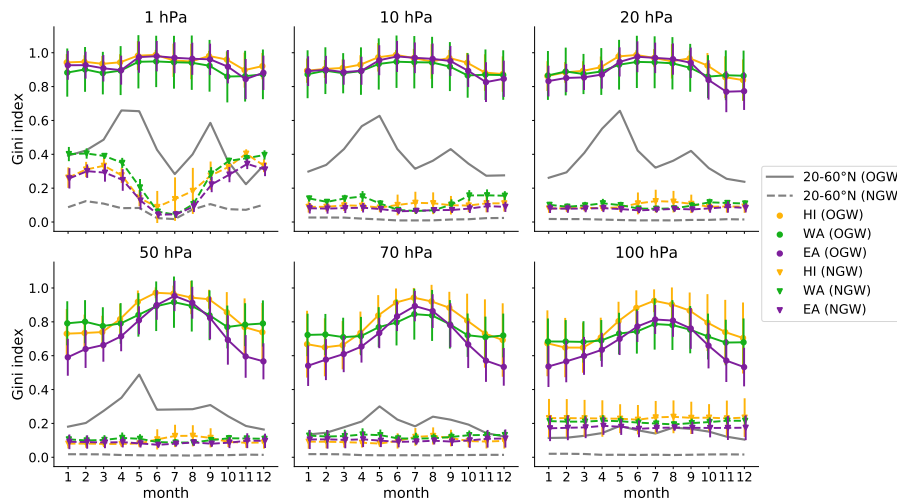


Figure 7. Spatial and annual variability of the Gini coefficient of GW momentum fluxes at 100, 70, 50, 20, 10, 1 hPa within the Himalaya, East Asia and West America hotspot, respectively. Solid lines with circles and dashed lines with triangles represent OGWs and NGWs, respectively. Gray lines denote the Gini coefficient calculated from zonal mean between 20 and 60°N. Error bars show the spatial standard deviation.

The composites of peak OGWD events within the hotspots naturally appear as statistically significant OGWD anomalies in the LS. The duration of the strong OGWD event differs slightly between the hotspots. For HI, OGWD anomalies are smaller than -1 m/s/day for 5 days prior to the peak. For WA and EA, we find significant OGWD anomalies within 2 or 3 days prior to the peak (lag=0). After the peak, strong OGWD anomalies occur up to +4 days for all hotspots. The vertical extent of the feature is similar in all three hotspots. For the HI and EA hotspots the OGWD anomaly reaches from about 100 hPa to 40 hPa with a statistically robust peak at 70 hPa. The WA hotspot has a slightly larger vertical extent. The strong OGWD events are also connected with statistically significant OGWD anomalies at higher altitudes. Above about 1 hPa, anomalously strong/weak OGWD for the WA/EA hotspot emerges. The OGWD anomalies in the upper stratosphere are negative but not significant for the HI hotspot. The enhanced westward OGWD results in a zonal-wind weakening in the mesosphere and is connected with zonal wind strengthening throughout the stratosphere (see contour lines in Fig. 8) except for EA, where we found zonal wind weakening throughout the stratosphere. This suggests that in the model the EA hotspot is connected with a critical level occurrence inhibiting further upward propagation of OGWs, while in the WA hotspot strong OGWD events are connected with strong momentum flux events. For the HI hotspot, the results are not conclusive due to the large variability of the strong OGWD events.

While we observe various anomalies above the hotspots between the upper stratosphere and the lower mesosphere (see Fig. 8), zonal-mean composites of OGWD reveal a common positive pattern. It indicates that the suppressed OGWD is connected with a weaker meridional residual circulation from lower to higher mesospheric latitudes. By the continuity equation, the weaker meridional transport is associated with weaker downward motion in polar latitudes which may result in a colder



Table 1. Number of detected peak events per month for the three selected hotspot areas. DJF values are emphasized.

	Himalayas	East Asia	West America
Month			
9	0	1	0
10	0	7	1
11	0	11	6
12	5	9	9
1	16	15	11
2	16	13	5
3	7	11	3
4	1	6	1
5	0	1	0

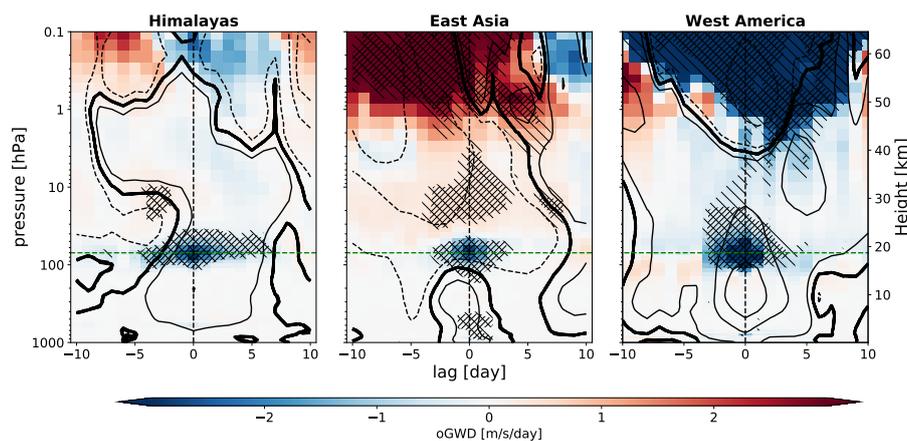


Figure 8. Composite anomalies of OGWD [m/s/day] averaged at all lags within the selected hotspot areas (Himalayas, East Asia and West America) on the 20-day timescale. Green lines represent the composite level, i.e. 70 hPa. Hatching $\backslash\backslash\backslash$ and $/\!/$ represents p-values < 0.05 and < 0.01 , respectively. Dashed and solid contour lines represent negative and positive zonal wind anomalies with amplitudes $\{\pm 1, \pm 5, \pm 8\}$ m/s within the selected hotspot, respectively. Solid bold line contours the zero-wind anomaly.



mesosphere (Zülicke et al., 2018). The positive OGWD anomalies reported here are similar as reported in Albers and Birner
280 (2014) and in Song and Chun (2016), i.e. suppressed in the regions of weak winds before the displacement SSWs. Hence,
there are potential links between the illustrated OGW hotspot composites and middle atmosphere dynamics and transport. For
example, the timing and the frequency of SSWs can be related to the GW forcing in the hotspots; and the upward propagation
of GWs into the mesosphere can be hindered. This way, the hotspot composites can have an impact on dynamics and transport
in the stratosphere. Analyses of these connections, however, go beyond the scope of the current paper and will be conducted in
285 a follow-up study.

4 Discussion and Conclusions

This study analyses the characteristics of parameterized OGWD in CMAM-sd with focus on the NH LS. The CMAM-sd
model output have been chosen for the analysis based on public availability of essential variables (OGW fluxes and drag) in 3D
and necessarily high temporal resolution. The present study is therefore also meant to constitute an example of open science
290 benefiting from publicly available 3D GW variables with high temporal resolution. The fact that CMAM-sd is nudged ensures
that the meteorological situation is close to reality, particularly in the LS, and therefore makes comparisons with observations
feasible. However, forcing the model dynamics also complicates the causal attribution of composite anomalies due to the two-
way interplay between the OGW forcing and the circulation in the middle atmosphere. In this study, we do not consider this
to be crucial, particularly, because the nudging is activated up to an altitude of 1 hPa only. We encourage modeling centres
295 to provide the GW diagnostics in three dimensions and with at least daily sampling to access the GWD intermittency also
for free running simulations. This information may help to improve the validation of model GW fluxes with observations and
consequent tuning of the drag strength.

Besides other known factors (e.g. neglect of horizontal propagation and directional absorption of GWs), different GW
intermittencies can contribute to the discrepancies of GW fluxes and drags between models and observational estimates, or
300 induce completely different impacts on the model atmospheres for "correct" zonal mean GWD climatologies. While the down-
ward control principle (Haynes et al., 1991) practiced in zonal mean is appropriate when studying momentum transfers by
large-scale waves for which the approximation by zonally symmetric torques is reasonable, it may not be appropriate for
studying atmospheric responses to momentum deposition associated with GWs (Shaw and Boos, 2012; Boos and Shaw, 2013).

We compared the zonal mean monthly mean OGW in the LS with reanalysis and observation-based data. This comparison
305 showed that the CMAM-sd OGWD and the OGW momentum fluxes are almost one order of magnitude larger than in observa-
tions. These differences may be explained by the fact that the parameterization of OGWs is tuned to represent a missing drag
in the SH resulting in the overestimation in the NH (McLandress et al., 2012). Using horizontal propagation and directional
absorption of OGWs in the parametrization may bring the GWD in the middle latitudes closer to observations (Xu et al., 2017,
2018), particularly considering that GW momentum fluxes as derived from satellite observations may be underestimated (Trinh
310 et al., 2015; Ern et al., 2018). Still, the high bias in the NH emerges as deficiency of current GW parameterizations in GCMs



in pursuit to eliminate the missing GWD near 60°S (McLandress et al., 2012) which is possibly associated with NGWs (Jewtougoff et al., 2015).

The OGWD probability density distribution can be approximated by a log-normal distribution. Within the selected hotspots (Himalayas, East Asia, West America) we can find extreme OGWD values exceeding -70m/s/day . After constructing one
315 representative timeseries for each hotspot by spatial averaging, the long tails of the distribution are reduced and we observe drag magnitudes of up to about -15m/s/day . Based on the Gini coefficient, we show that the hotspot averaged OGWD is highly intermittent and comparable with past observational studies (Alexander et al., 2016; Jewtougoff et al., 2015; Plougonven et al., 2013; Wright et al., 2013). For all hotspots the intermittency is induced predominantly by the near surface variability. However, the role of background flow variability in the LS also plays an important role, especially for EA, where near surface
320 momentum fluxes partly stipulate the annual cycle in the stratosphere.

By means of the information of the spatio-temporal distribution of OGWD, we develop a method to study the impact of localized peak OGWD events in the three selected hotspot areas. The peak-detection method is based on local OGWD minima and therefore independent of the high bias outlined above. We construct composites of peak OGWD events at 70hPa and apply the method to spatially averaged OGWD profiles connected with the particular hotspots to obtain information on duration and
325 vertical structure of the strong OGWD events. This helps us to infer the nature of those events. The assumption of vertically propagating GWs applied in model parameterizations seems to be realistic in the LS (see Fig. 7, Kalisch et al., 2014) which enhances confidence in our composites. One of the key results of our study is that LS peak OGW events can have opposing effects on the upper stratosphere and mesosphere depending on the hotspot region. Taking a zonal-mean perspective reveals that positive OGWD anomalies contribute to mesospheric cooling (Zülicke et al., 2018) when stratospheric winds weaken.

330 The analysis presented in this study constitutes a new method for studying the intermittency of OGWs, especially in hotspot regions, where the intermittency was shown to be large. Additionally, the composite analysis constitutes a new possibility to analyze the effect of the OGW hotspot regions on middle atmospheric dynamics, widening our understanding of the effects of GWs on dynamics and transport.

Code and data availability. All processed data for this study are provided via the Mendeley Data (Kuchar, 2020b). All and codes to re-
335 produce our figures are provided via Github (Kuchar, 2020a). The authors would like to thank to all colleagues involved in the CMAM-sd model simulation (obtained from: <http://climate-modelling.canada.ca/climatemodeldata/cmam/output/CMAM/CMAM30-SD/index.shtml>); reanalyses: MERRA2 (obtained from <http://disc.sci.gsfc.nasa.gov/daac-bin/FTPSubset2.pl>) and JRA55 (obtained from http://jra.kishou.go.jp/JRA-55/index_en.html); S-RIP diagnostics (Martineau, 2017); and observations: GRACILE (obtained from <https://doi.org/10.1594/PANGAEA.879658>). Furthermore, we acknowledge developers of python open-source software libraries used for this paper: *aostools* (Jucker,
340 2018), *cartopy* (Met Office, 2010 - 2015), *detecta* (Duarte, 2020), *matplotlib* (Hunter, 2007), *numpy* (Oliphant, 2006), *pandas* (McKinney, 2010), *seaborn* (Waskom et al., 2016), *scipy* (Virtanen et al., 2020), *xarray* (Hoyer et al., 2016) and *xclim* (Huard et al., 2020)



Author contributions. AK and PS designed the study. AK analysed the data. AK, PS and RE compiled the manuscript with inputs of other authors.

Competing interests. The authors declare that they have no conflict of interest.

345 *Acknowledgements.* AK and CJ acknowledge support from Deutsche Forschungsgemeinschaft under grant JA836/43-1 (VACILT). PS is supported through the project CZ.02.2.69/0.0/0.0/19_074/0016231 (International mobility of researchers at Charles University (MSCA-IF III)) for the research stay at BOKU Vienna and at earlier stages of the manuscript by a postdoctoral grant of Xunta de Galicia ED481B 2018/103. RE was funded by the Helmholtz Association under grant VH-NG-1014 (Helmholtz-Hochschul-Nachwuchsforschergruppe MAClim). RE and PS acknowledge support from the BTHA under grant number BTHA-MOB-2020-2. Further, PS would like to acknowledge discussions
350 at the ISSI Bern with members of the New Quantitative Constraints on Orographic Gravity Wave Stress and Drag Satisfying Emerging Needs in Seasonal-to-Subseasonal and Climate Prediction. Foundations of this study was laid during projects supported by GA CR under grant nos. 16-01562J and 18-01625S.



References

- Abalos, M., Legras, B., Ploeger, F., and Randel, W. J.: Evaluating the advective Brewer-Dobson circulation in three reanalyses for the period
355 1979-2012, *Journal of Geophysical Research: Atmospheres*, 120, 7534–7554, <https://doi.org/10.1002/2015JD023182>, <http://doi.wiley.com/10.1002/2015JD023182>, 2015.
- Albers, J. R. and Birner, T.: Vortex Preconditioning due to Planetary and Gravity Waves prior to Sudden Stratospheric Warmings, *Journal of the Atmospheric Sciences*, 71, 4028–4054, <https://doi.org/10.1175/JAS-D-14-0026.1>, <http://journals.ametsoc.org/doi/abs/10.1175/JAS-D-14-0026.1>, 2014.
- 360 Alexander, M. J.: Gravity Waves in the Stratosphere, pp. 109–121, American Geophysical Union (AGU), <https://doi.org/10.1002/9781118666630.ch6>, <https://agupubs.onlinelibrary.wiley.com/doi/abs/10.1002/9781118666630.ch6>, 2013.
- Alexander, S. P., Sato, K., Watanabe, S., Kawatani, Y., and Murphy, D. J.: Southern Hemisphere Extratropical Gravity Wave Sources and Intermittency Revealed by a Middle-Atmosphere General Circulation Model, *Journal of the Atmospheric Sciences*, 73, 1335–1349, <https://doi.org/10.1175/JAS-D-15-0149.1>, <http://journals.ametsoc.org/doi/10.1175/JAS-D-15-0149.1>, 2016.
- 365 Andrews, D. G. and McIntyre, M. E.: JR Holton, and CB Leovy, 1987: *Middle Atmosphere Dynamics*, 1987.
- Boos, W. R. and Shaw, T. A.: The effect of moist convection on the tropospheric response to tropical and subtropical zonally asymmetric torques, *Journal of the Atmospheric Sciences*, 70, 4089–4111, <https://doi.org/10.1175/JAS-D-13-041.1>, <https://doi.org/10.1175/JAS-D-13-041.1>, 2013.
- Bramberger, M., Dörnbrack, A., Bossert, K., Ehard, B., Fritts, D. C., Kaifler, B., Mallaun, C., Orr, A., Pautet, P.-D., Rapp, M., Taylor, M. J.,
370 Vosper, S., Williams, B. P., and Witschas, B.: Does Strong Tropospheric Forcing Cause Large-Amplitude Mesospheric Gravity Waves? A DEEPWAVE Case Study, *Journal of Geophysical Research: Atmospheres*, 122, 11,422–11,443, <https://doi.org/10.1002/2017JD027371>, <http://doi.wiley.com/10.1002/2017JD027371>, 2017.
- Cao, B. and Liu, A. Z.: Intermittency of gravity wave momentum flux in the mesopause region observed with an all-sky airglow imager, *Journal of Geophysical Research: Atmospheres*, 121, 650–663, <https://doi.org/10.1002/2015JD023802>, <https://agupubs.onlinelibrary.wiley.com/doi/abs/10.1002/2015JD023802>, 2016.
- 375 Charlton, A. J. and Polvani, L. M.: A New Look at Stratospheric Sudden Warmings. Part I: Climatology and Modeling Benchmarks, *Journal of Climate*, 20, 449–469, <https://doi.org/10.1175/JCLI3996.1>, <http://journals.ametsoc.org/doi/abs/10.1175/JCLI3996.1>, 2007.
- Chun, H.-y., Song, B.-G., Shin, S.-W., and Kim, Y.-H.: Gravity Waves Associated with Jet/Front Systems. Part I: Diagnostics and their Correlations with GWs Revealed in High-Resolution Global Analysis Data, *Asia-Pacific Journal of Atmospheric Sciences*, 55, 589–608,
380 <https://doi.org/10.1007/s13143-019-00104-1>, <http://link.springer.com/10.1007/s13143-019-00104-1>, 2019.
- Cohen, N. Y. and Boos, W. R.: The influence of orographic Rossby and gravity waves on rainfall, *Quarterly Journal of the Royal Meteorological Society*, 143, 845–851, <https://doi.org/10.1002/qj.2969>, 2017.
- Dee, D. P., Uppala, S. M., Simmons, A. J., Berrisford, P., Poli, P., Kobayashi, S., Andrae, U., Balmaseda, M. A., Balsamo, G., Bauer, P., Bechtold, P., Beljaars, A. C. M., van de Berg, L., Bidlot, J., Bormann, N., Delsol, C., Dragani, R., Fuentes, M., Geer, A. J., Haimberger, L., Healy, S. B., Hersbach, H., Hólm, E. V., Isaksen, L., Kållberg, P., Köhler, M., Matricardi, M., McNally, A. P., Monge-Sanz, B. M., Morcrette, J.-J., Park, B.-K., Peubey, C., de Rosnay, P., Tavolato, C., Thépaut, J.-N., and Vitart, F.: The ERA-Interim reanalysis: configuration and performance of the data assimilation system, *Quarterly Journal of the Royal Meteorological Society*, 137, 553–597, <https://doi.org/10.1002/qj.828>, <http://doi.wiley.com/10.1002/qj.828>, 2011.



- Dietmüller, S., Eichinger, R., Garny, H., Birner, T., Boenisch, H., Pitari, G., Mancini, E., Visionsi, D., Stenke, A., Revell, L., Rozanov, E.,
390 Plummer, D. A., Scinocca, J., Jöckel, P., Oman, L., Deushi, M., Kiyotaka, S., Kinnison, D. E., Garcia, R., Morgenstern, O., Zeng, G., Stone,
K. A., and Schofield, R.: Quantifying the effect of mixing on the mean age of air in CCMVal-2 and CCMI-1 models, *Atmospheric Chem-
istry and Physics*, 18, 6699–6720, <https://doi.org/10.5194/acp-18-6699-2018>, <https://www.atmos-chem-phys.net/18/6699/2018/>, 2018.
- Duarte, M.: detecta: A Python module to detect events in data, <https://github.com/demotu/detecta>, 2020.
- Ebita, A., Kobayashi, S., Ota, Y., Moriya, M., Kumabe, R., Onogi, K., Harada, Y., Yasui, S., Miyaoka, K., Takahashi, K., Kamahori, H.,
395 Kobayashi, C., Endo, H., Soma, M., Oikawa, Y., and Ishimizu, T.: The Japanese 55-year Reanalysis (JRA-55): an interim report, *Sola*, 7,
149–152, <https://doi.org/10.2151/sola.2011-038>, <https://doi.org/10.2151/sola.2011-038>, 2011.
- Ehard, B., Kaifler, B., Dörnbrack, A., Preusse, P., Eckermann, S. D., Bramberger, M., Gisinger, S., Kaifler, N., Liley, B., Wagner, J., and
Rapp, M.: Horizontal propagation of large-amplitude mountain waves into the polar night jet, *Journal of Geophysical Research*, 122,
1423–1436, <https://doi.org/10.1002/2016JD025621>, 2017.
- 400 Ern, M., Trinh, Q. T., Preusse, P., Gille, J. C., Mlynczak, M. G., Russell III, J. M., and Riese, M.: GRACILE: a comprehensive
climatology of atmospheric gravity wave parameters based on satellite limb soundings, *Earth System Science Data*, 10, 857–892,
<https://doi.org/10.5194/essd-10-857-2018>, <https://www.earth-syst-sci-data.net/10/857/2018/>, 2018.
- Fritts, D. C. and Alexander, M. J.: Gravity wave dynamics and effects in the middle atmosphere, *Reviews of Geophysics*, 41,
<https://doi.org/10.1029/2001RG000106>, <https://agupubs.onlinelibrary.wiley.com/doi/abs/10.1029/2001RG000106>, 2003.
- 405 Fujiwara, M., Wright, J. S., Manney, G. L., Gray, L. J., Anstey, J., Birner, T., Davis, S., Gerber, E. P., Harvey, V. L., Hegglin, M. I., Home-
yer, C. R., Knox, J. A., Krüger, K., Lambert, A., Long, C. S., Martineau, P., Molod, A., Monge-Sanz, B. M., Santee, M. L., Tegtmeier,
S., Chabrillat, S., Tan, D. G. H., Jackson, D. R., Polavarapu, S., Compo, G. P., Dragani, R., Ebisuzaki, W., Harada, Y., Kobayashi,
C., McCarty, W., Onogi, K., Pawson, S., Simmons, A., Wargan, K., Whitaker, J. S., and Zou, C.-Z.: Introduction to the SPARC Re-
analysis Intercomparison Project (S-RIP) and overview of the reanalysis systems, *Atmospheric Chemistry and Physics*, 17, 1417–1452,
410 <https://doi.org/10.5194/acp-17-1417-2017>, <https://www.atmos-chem-phys.net/17/1417/2017/>, 2017.
- Garcia, R. R. and Boville, B. A.: "Downward Control" of the Mean Meridional Circulation and Temperature Distribu-
tion of the Polar Winter Stratosphere, *Journal of the Atmospheric Sciences*, 51, 2238–2245, [https://doi.org/10.1175/1520-0469\(1994\)051<2238:COTMMC>2.0.CO;2](https://doi.org/10.1175/1520-0469(1994)051<2238:COTMMC>2.0.CO;2), [https://doi.org/10.1175/1520-0469\(1994\)051<2238:COTMMC>2.0.CO;2](https://doi.org/10.1175/1520-0469(1994)051<2238:COTMMC>2.0.CO;2), 1994.
- Garcia, R. R., Smith, A. K., Kinnison, D. E., de la Cámara, Á., and Murphy, D. J.: Modification of the Gravity Wave Parameterization
415 in the Whole Atmosphere Community Climate Model: Motivation and Results, *Journal of the Atmospheric Sciences*, 74, 275–291,
<https://doi.org/10.1175/JAS-D-16-0104.1>, <http://journals.ametsoc.org/doi/10.1175/JAS-D-16-0104.1>, 2017.
- Geller, M. A., Alexander, M. J., Love, P. T., Bacmeister, J., Ern, M., Hertzog, A., Manzini, E., Preusse, P., Sato, K., Scaife, A. A., and Zhou,
T.: A Comparison between Gravity Wave Momentum Fluxes in Observations and Climate Models, *Journal of Climate*, 26, 6383–6405,
<https://doi.org/10.1175/JCLI-D-12-00545.1>, <http://journals.ametsoc.org/doi/abs/10.1175/JCLI-D-12-00545.1>, 2013.
- 420 Gini, C.: Italian: Variabilità e mutabilità, Variability and Mutability', C. Cuppini, Bologna, 1912.
- Haynes, P. H., McIntyre, M. E., Shepherd, T. G., Marks, C. J., and Shine, K. P.: On the "Downward Control" of Ex-
tratropical Diabatic Circulations by Eddy-Induced Mean Zonal Forces, *Journal of the Atmospheric Sciences*, 48, 651–
678, [https://doi.org/10.1175/1520-0469\(1991\)048<0651:OTCOED>2.0.CO;2](https://doi.org/10.1175/1520-0469(1991)048<0651:OTCOED>2.0.CO;2), [http://journals.ametsoc.org/doi/abs/10.1175/1520-0469\(1991\)048<0651:OTCOED>2.0.CO;2](http://journals.ametsoc.org/doi/abs/10.1175/1520-0469(1991)048<0651:OTCOED>2.0.CO;2), 1991.



- 425 Hertzog, A., Alexander, M. J., and Plougonven, R.: On the Intermittency of Gravity Wave Momentum Flux in the Stratosphere, *Journal of the Atmospheric Sciences*, 69, 3433–3448, <https://doi.org/10.1175/JAS-D-12-09.1>, <http://journals.ametsoc.org/doi/abs/10.1175/JAS-D-12-09.1>, 2012.
- Hoffmann, L., Xue, X., and Alexander, M. J.: A global view of stratospheric gravity wave hotspots located with Atmospheric Infrared Sounder observations, *Journal of Geophysical Research: Atmospheres*, 118, 416–434, <https://doi.org/10.1029/2012JD018658>, <http://doi.wiley.com/10.1029/2012JD018658>, 2013.
- 430 Hoyer, S., Fitzgerald, C., Hamman, J., akleeman, Kluyver, T., Roos, M., Helmus, J. J., Markel, Cable, P., Maussion, F., Miles, A., Kanmae, T., Wolfram, P., Sinclair, S., Bovy, B., ebrevdo, Guedes, R., Abernathey, R., Filipe, Hill, S., Richards, N., Lee, A., Koldunov, N., Graham, M., maciekswat, Gerard, J., Babuschkin, I., Deil, C., Welch, E., and Hilboll, A.: xarray: v0.8.0, <https://doi.org/10.5281/zenodo.59499>, 2016.
- 435 Huard, D., Smith, T. J., Logan, T., Bourgault, P., sbiner, Caron, D., Roy, P., jwenfai, RondeauG, Whelan, C., and Stephens, A.: Ouranos-inc/xclim: v0.15.0, <https://doi.org/10.5281/zenodo.3708391>, <https://doi.org/10.5281/zenodo.3708391>, 2020.
- Hunter, J. D.: Matplotlib: A 2D graphics environment, *Computing In Science & Engineering*, 9, 90–95, 2007.
- Iwasaki, T., Yamada, S., and Tada, K.: A parameterization scheme of orographic gravity wave drag with two different vertical partitionings, *Journal of the Meteorological Society of Japan. Ser. II*, 67, 11–27, 1989.
- 440 Jewtoukoff, V., Hertzog, A., Plougonven, R., Cámara, A. d. I., and Lott, F.: Comparison of gravity waves in the Southern Hemisphere derived from balloon observations and the ECMWF analyses, *Journal of the Atmospheric Sciences*, 72, 3449–3468, <https://doi.org/10.1175/JAS-D-14-0324.1>, <http://journals.ametsoc.org/doi/10.1175/JAS-D-14-0324.1>, 2015.
- Jucker, M.: mjucker/aostools: aostools v2.1.5, <https://doi.org/10.5281/zenodo.1252733>, <https://doi.org/10.5281/zenodo.1252733>, 2018.
- Kalisch, S., Preusse, P., Ern, M., Eckermann, S. D., and Riese, M.: Differences in gravity wave drag between realistic oblique and assumed vertical propagation, *Journal of Geophysical Research: Atmospheres*, 119, 10,081–10,099, <https://doi.org/10.1002/2014JD021779>, <http://doi.wiley.com/10.1002/2014JD021779>, 2014.
- 445 Kendall, M. and Stuart, A.: *The advanced theory of statistics. Vol. 1: Distribution theory*, London: Griffin, 1977, 4th ed., 1977.
- Kruse, C. G., Smith, R. B., and Eckermann, S. D.: The Midlatitude Lower-Stratospheric Mountain Wave "Valve Layer", *Journal of the Atmospheric Sciences*, 73, 5081–5100, <https://doi.org/10.1175/JAS-D-16-0173.1>, <https://doi.org/10.1175/JAS-D-16-0173.1>, 2016.
- 450 Kuchar, A.: kuchaale/wcd_2020: First release of my WCD code repository, <https://doi.org/10.5281/zenodo.3780102>, https://github.com/kuchaale/wcd_2020, 2020a.
- Kuchar, A.: Accompanying data to "On the intermittency of orographic gravity wave hotspots and its importance for middle atmosphere dynamics", <https://doi.org/10.17632/j3hj7f9t67.1>, 2020b.
- Kuilman, M., Karlsson, B., Benze, S., and Megner, L.: Exploring noctilucent cloud variability using the nudged and extended version of the Canadian Middle Atmosphere Model, *Journal of Atmospheric and Solar-Terrestrial Physics*, 164, 276–288, <https://doi.org/10.1016/j.jastp.2017.08.019>, <https://doi.org/10.1016/j.jastp.2017.08.019><http://linkinghub.elsevier.com/retrieve/pii/S1364682617301529>, 2017.
- 455 Martineau, P.: S-RIP: Zonal-mean dynamical variables of global atmospheric reanalyses on pressure levels, <https://doi.org/10.5285/b241a7f536a244749662360bd7839312>, 2017.
- 460 Martineau, P., Son, S.-W., and Taguchi, M.: Dynamical Consistency of Reanalysis Datasets in the Extratropical Stratosphere, *Journal of Climate*, 29, 3057–3074, <https://doi.org/10.1175/JCLI-D-15-0469.1>, <http://journals.ametsoc.org/doi/10.1175/JCLI-D-15-0469.1>, 2016.



- McFarlane, N. A.: The Effect of Orographically Excited Gravity Wave Drag on the General Circulation of the Lower Stratosphere and Troposphere, *Journal of the Atmospheric Sciences*, 44, 1775–1800, [https://doi.org/10.1175/1520-0469\(1987\)044<1775:TEOOEG>2.0.CO;2](https://doi.org/10.1175/1520-0469(1987)044<1775:TEOOEG>2.0.CO;2), [http://journals.ametsoc.org/doi/abs/10.1175/1520-0469\(1987\)044<1775:TEOOEG>2.0.CO;2](http://journals.ametsoc.org/doi/abs/10.1175/1520-0469(1987)044<1775:TEOOEG>2.0.CO;2), 1987.
- McKinney, W.: Data Structures for Statistical Computing in Python, in: *Proceedings of the 9th Python in Science Conference*, edited by van der Walt, S. and Millman, J., pp. 51 – 56, 2010.
- McLandress, C., Shepherd, T. G., Polavarapu, S., and Beagley, S. R.: Is Missing Orographic Gravity Wave Drag near 60°S the Cause of the Stratospheric Zonal Wind Biases in Chemistry-Climate Models?, *Journal of the Atmospheric Sciences*, 69, 802–818, <https://doi.org/10.1175/JAS-D-11-0159.1>, <http://journals.ametsoc.org/doi/abs/10.1175/JAS-D-11-0159.1>, 2012.
- McLandress, C., Scinocca, J. F., Shepherd, T. G., Reader, M. C., and Manney, G. L.: Dynamical Control of the Mesosphere by Orographic and Nonorographic Gravity Wave Drag during the Extended Northern Winters of 2006 and 2009, *Journal of the Atmospheric Sciences*, 70, 2152–2169, <https://doi.org/10.1175/JAS-D-12-0297.1>, <http://journals.ametsoc.org/doi/abs/10.1175/JAS-D-12-0297.1>, 2013.
- McLandress, C., Plummer, D. A., and Shepherd, T. G.: Technical Note: A simple procedure for removing temporal discontinuities in ERA-Interim upper stratospheric temperatures for use in nudged chemistry-climate model simulations, *Atmospheric Chemistry and Physics*, 14, 1547–1555, <https://doi.org/10.5194/acp-14-1547-2014>, <http://www.atmos-chem-phys.net/14/1547/2014/>, 2014.
- Met Office: Cartopy: a cartographic python library with a matplotlib interface, Exeter, Devon, <http://scitools.org.uk/cartopy>, 2010 - 2015.
- Molod, A., Takacs, L., Suarez, M., and Bacmeister, J.: Development of the GEOS-5 atmospheric general circulation model: evolution from MERRA to MERRA2, *Geoscientific Model Development*, 8, 1339–1356, <https://doi.org/10.5194/gmd-8-1339-2015>, <http://www.geosci-model-dev.net/8/1339/2015/><https://disc.sci.gsfc.nasa.gov/daac-bin/FTPSubset2.pl>, 2015.
- Nakamura, H., Miyasaka, T., Kosaka, Y., Takaya, K., and Honda, M.: Northern Hemisphere Extratropical Tropospheric Planetary Waves and their Low-Frequency Variability: Their Vertical Structure and Interaction with Transient Eddies and Surface Thermal Contrasts, *Climate Dynamics: Why Does Climate Vary*, pp. 149–179, <https://doi.org/10.1029/2008GM000789>, 2013.
- Okamoto, K., Sato, K., and Akiyoshi, H.: A study on the formation and trend of the Brewer-Dobson circulation, *Journal of Geophysical Research: Atmospheres*, 116, <https://doi.org/10.1029/2010JD014953>, <https://agupubs.onlinelibrary.wiley.com/doi/abs/10.1029/2010JD014953>, 2011.
- Oliphant, T. E.: *A guide to NumPy*, vol. 1, Trelgol Publishing USA, 2006.
- Pendlebury, D., Plummer, D., Scinocca, J., Sheese, P., Strong, K., Walker, K., and Degenstein, D.: Comparison of the CMAM30 data set with ACE-FTS and OSIRIS: polar regions, *Atmospheric Chemistry and Physics*, 15, 12465–12485, <https://doi.org/10.5194/acp-15-12465-2015>, <http://www.atmos-chem-phys.net/15/12465/2015/>, 2015.
- Pisoft, P., Sacha, P., Miksovsky, J., Huszar, P., Scherllin-Pirscher, B., and Foelsche, U.: Revisiting internal gravity waves analysis using GPS RO density profiles: comparison with temperature profiles and application for wave field stability study, *Atmospheric Measurement Techniques*, 11, 515–527, <https://doi.org/10.5194/amt-11-515-2018>, <https://www.atmos-meas-tech.net/11/515/2018/>, 2018.
- Plougonven, R. and Zhang, F.: Internal gravity waves from atmospheric jets and fronts, *Reviews of Geophysics*, 52, 33–76, <https://doi.org/10.1002/2012RG000419>, <http://doi.wiley.com/10.1002/2012RG000419>, 2014.
- Plougonven, R., Hertzog, A., and Guez, L.: Gravity waves over Antarctica and the Southern Ocean: Consistent momentum fluxes in mesoscale simulations and stratospheric balloon observations, *Quarterly Journal of the Royal Meteorological Society*, 139, 101–118, 2013.
- Plumb, R. A.: Stratospheric Transport, *Journal of the Meteorological Society of Japan. Ser. II*, 80, 793–809, <https://doi.org/10.2151/jmsj.80.793>, [https://www.jstage.jst.go.jp/article/jmsj/80/4B/80\(4B\)793/article](https://www.jstage.jst.go.jp/article/jmsj/80/4B/80(4B)793/article), 2002.



- 500 Šácha, P., Kuchar, A., Jacobi, C., and Pišoft, P.: Enhanced internal gravity wave activity and breaking over the northeastern Pacific-eastern Asian region, *Atmospheric Chemistry and Physics*, 15, 13 097–13 112, <https://doi.org/10.5194/acp-15-13097-2015>, <http://www.atmos-chem-phys.net/15/13097/2015/>, 2015.
- Sato, K. and Hirano, S.: The climatology of the Brewer–Dobson circulation and the contribution of gravity waves, *Atmospheric Chemistry and Physics*, 19, 4517–4539, <https://doi.org/10.5194/acp-19-4517-2019>, <https://www.atmos-chem-phys.net/19/4517/2019/>, 2019.
- 505 Scheffler, G. and Pulido, M.: Compensation between Resolved and Unresolved Wave Drag in the Stratospheric Final Warmings of the Southern Hemisphere, *Journal of the Atmospheric Sciences*, 72, 4393–4411, <https://doi.org/10.1175/JAS-D-14-0270.1>, <http://journals.ametsoc.org/doi/10.1175/JAS-D-14-0270.1>, 2015.
- Scinocca, J. F.: An Accurate Spectral Nonorographic Gravity Wave Drag Parameterization for General Circulation Models, *Journal of the Atmospheric Sciences*, 60, 667–682, [https://doi.org/10.1175/1520-0469\(2003\)060<0667:AASNGW>2.0.CO;2](https://doi.org/10.1175/1520-0469(2003)060<0667:AASNGW>2.0.CO;2), [http://journals.ametsoc.org/doi/abs/10.1175/1520-0469\(2003\)060<0667:AASNGW>2.0.CO;2](http://journals.ametsoc.org/doi/abs/10.1175/1520-0469(2003)060<0667:AASNGW>2.0.CO;2), 2003.
- 510 Scinocca, J. F. and McFarlane, N. A.: The parametrization of drag induced by stratified flow over anisotropic orography, *Quarterly Journal of the Royal Meteorological Society*, 126, 2353–2393, <https://doi.org/10.1002/qj.49712656802>, <http://doi.wiley.com/10.1002/qj.49712656802>, 2000.
- Scinocca, J. F., McFarlane, N. A., Lazare, M., Li, J., and Plummer, D.: Technical Note: The CCCma third generation AGCM and its extension
515 into the middle atmosphere, *Atmospheric Chemistry and Physics*, 8, 7055–7074, <https://doi.org/10.5194/acp-8-7055-2008>, <http://www.atmos-chem-phys.net/8/7055/2008/>, 2008.
- Seviour, W. J., Butchart, N., and Hardiman, S. C.: The Brewer–Dobson circulation inferred from ERA-Interim, *Quarterly Journal of the Royal Meteorological Society*, 138, 878–888, 2012.
- Seviour, W. J. M., Mitchell, D. M., and Gray, L. J.: A practical method to identify displaced and split stratospheric polar vortex events,
520 *Geophysical Research Letters*, 40, 5268–5273, <https://doi.org/10.1002/grl.50927>, <http://doi.wiley.com/10.1002/grl.50927>, 2013.
- Shaw, T. A. and Boos, W. R.: The Tropospheric Response to Tropical and Subtropical Zonally Asymmetric Torques: Analytical and Idealized Numerical Model Results, *Journal of the Atmospheric Sciences*, 69, 214–235, <https://doi.org/10.1175/JAS-D-11-0139.1>, <http://journals.ametsoc.org/doi/abs/10.1175/JAS-D-11-0139.1>, 2012.
- Shepherd, T. G., Plummer, D. A., Scinocca, J. F., Hegglin, M. I., Fioletov, V. E., Reader, M. C., Remsberg, E., Von Clarmann, T.,
525 and Wang, H. J.: Reconciliation of halogen-induced ozone loss with the total-column ozone record, *Nature Geoscience*, 7, 443–449, <https://doi.org/10.1038/ngeo2155>, 2014.
- Song, B.-G. and Chun, H.-Y.: Residual Mean Circulation and Temperature Changes during the Evolution of Stratospheric Sudden Warming Revealed in MERRA, *Atmospheric Chemistry and Physics Discussions*, 2016, 1–26, <https://doi.org/10.5194/acp-2016-729>, <https://www.atmos-chem-phys-discuss.net/acp-2016-729/>, 2016.
- 530 Stephan, C. C., Schmidt, H., Zülicke, C., and Matthias, V.: Oblique Gravity Wave Propagation During Sudden Stratospheric Warmings, *Journal of Geophysical Research: Atmospheres*, 125, e2019JD031 528, <https://doi.org/10.1029/2019JD031528>, <https://agupubs.onlinelibrary.wiley.com/doi/abs/10.1029/2019JD031528>, e2019JD031528 10.1029/2019JD031528, 2020.
- Teixeira, M. A.: The physics of orographic gravity wave drag, *Frontiers in Physics*, 2, 43, 2014.
- Trinh, Q., Kalisch, S., Preusse, P., Chun, H.-Y., Eckermann, S. D., Ern, M., and Riese, M.: A comprehensive observational filter for satellite
535 infrared limb sounding of gravity waves, *Atmospheric measurement techniques*, 8, 1491–1517, 2015.



- van Niekerk, A., Sandu, I., and Vosper, S. B.: The Circulation Response to Resolved Versus Parametrized Orographic Drag Over Complex Mountain Terrains, *Journal of Advances in Modeling Earth Systems*, 10, 2527–2547, <https://doi.org/10.1029/2018MS001417>, <https://agupubs.onlinelibrary.wiley.com/doi/abs/10.1029/2018MS001417>, 2018.
- 540 Virtanen, P., Gommers, R., Oliphant, T. E., Haberland, M., Reddy, T., Cournapeau, D., Burovski, E., Peterson, P., Weckesser, W., Bright, J., van der Walt, S. J., Brett, M., Wilson, J., Jarrod Millman, K., Mayorov, N., Nelson, A. R. J., Jones, E., Kern, R., Larson, E., Carey, C., Polat, İ., Feng, Y., Moore, E. W., Vand erPlas, J., Laxalde, D., Perktold, J., Cimrman, R., Henriksen, I., Quintero, E. A., Harris, C. R., Archibald, A. M., Ribeiro, A. H., Pedregosa, F., van Mulbregt, P., and Contributors, S. . . : SciPy 1.0: Fundamental Algorithms for Scientific Computing in Python, *Nature Methods*, 17, 261–272, <https://doi.org/10.1038/s41592-019-0686-2>, 2020.
- 545 Šácha, P., Miksovsky, J., and Pisoft, P.: Interannual variability in the gravity wave drag – vertical coupling and possible climate links, *Earth System Dynamics*, 9, 647–661, <https://doi.org/10.5194/esd-9-647-2018>, <https://www.earth-syst-dynam.net/9/647/2018/>, 2018.
- Šácha, P., Eichinger, R., Garny, H., Pišoft, P., Dietmüller, S., de la Torre, L., Plummer, D. A., Jöckel, P., Morgenstern, O., Zeng, G., Butchart, N., and Añel, J. A.: Extratropical Age of Air trends and causative factors in climate projection simulations, *Atmospheric Chemistry and Physics Discussions*, 2019, 1–37, <https://doi.org/10.5194/acp-2018-1310>, <https://www.atmos-chem-phys-discuss.net/acp-2018-1310/>, 2019.
- 550 Waskom, M., Botvinnik, O., drewokane, Hobson, P., David, Halchenko, Y., Lukauskas, S., Cole, J. B., Warmenhoven, J., de Ruiter, J., Hoyer, S., Vanderplas, J., Villalba, S., Kunter, G., Quintero, E., Martin, M., Miles, A., Meyer, K., Augspurger, T., Yarkoni, T., Bachant, P., Williams, M., Evans, C., Fitzgerald, C., Brian, Wehner, D., Hitz, G., Ziegler, E., Qalieh, A., and Lee, A.: seaborn: v0.7.1 (June 2016), <https://doi.org/10.5281/zenodo.54844>, 2016.
- White, R. H., Battisti, D. S., and Sheshadri, A.: Orography and the Boreal Winter Stratosphere: The Importance of the Mongolian Mountains, *Geophysical Research Letters*, 45, 2088–2096, <https://doi.org/10.1002/2018GL077098>, <http://doi.wiley.com/10.1002/2018GL077098>, 2018.
- Wright, C. J., Osprey, S. M., and Gille, J. C.: Global observations of gravity wave intermittency and its impact on the observed momentum flux morphology, *Journal of Geophysical Research: Atmospheres*, 118, 10–980–10,993, <https://doi.org/10.1002/jgrd.50869>, <https://agupubs.onlinelibrary.wiley.com/doi/abs/10.1002/jgrd.50869>, 2013.
- 560 Xu, X., Wang, Y., Xue, M., and Zhu, K.: Impacts of Horizontal Propagation of Orographic Gravity Waves on the Wave Drag in the Stratosphere and Lower Mesosphere, *Journal of Geophysical Research: Atmospheres*, 122, 11,301–11,312, <https://doi.org/10.1002/2017JD027528>, <http://doi.wiley.com/10.1002/2017JD027528>, 2017.
- Xu, X., Tang, Y., Wang, Y., and Xue, M.: Directional Absorption of Parameterized Mountain Waves and Its Influence on the Wave Momentum Transport in the Northern Hemisphere, *Journal of Geophysical Research: Atmospheres*, pp. 1–15, <https://doi.org/10.1002/2017JD027968>, 565 <http://doi.wiley.com/10.1002/2017JD027968>, 2018.
- Zülicke, C., Becker, E., Matthias, V., Peters, D. H., Schmidt, H., Liu, H.-L., Ramos, L. d. l. T., and Mitchell, D. M.: Coupling of stratospheric warmings with mesospheric coolings in observations and simulations, *Journal of Climate*, 31, 1107–1133, 2018.